(peer-reviewed and in press in *Science Advances*)

Secular change of true polar wander over the past billion years

Authors: Hairuo Fu[1,2], Shihong Zhang[1]*, Daniel J. Condon[3], Hanbiao Xian[1]

Affiliations:

[1]State Key Laboratory of Biogeology and Environmental Geology, China University of Geosciences, Beijing 100083, China.
[2]Department of Earth and Planetary Sciences, Harvard University, MA 02138, USA.
[3]NERC Isotope Geosciences Laboratory, British Geological Survey, Keyworth NG12 5GG, UK.

*Corresponding author email: shzhang@cugb.edu.cn

Abstract:

The rate of movement of Earth's solid shell relative to its spin axis, or true polar wander, depends on variations in mantle convection and viscosity. We report paleomagnetic and geochronologic data from South China that constrain the rate of rapid true polar wander (>5° Myr^{-1}) from 832–821 million years ago. Analysis of the paleomagnetic database demonstrates secular change of true polar wander related to mantle cooling and thermal structure across supercontinent cycles. True polar wander rates are relatively muted with a partially insulated mantle during supercontinent assembly and accelerate as mantle thermal mixing re-establishes with supercontinent breakup. Decreasing true polar wander rate through the Neoproterozoic was succeeded by smaller variations in the Phanerozoic. We propose that extensive Neoproterozoic plate-tectonic activities enhanced mantle cooling, giving rise to a reduction in mantle convective forcing, an increase in mantle viscosity, and a decrease in true polar wander rates into the Phanerozoic.

One Sentence Summary:
Mantle cooling and thermal structure control secular change of true polar wander rates.

Introduction

True polar wander (TPW) is the rotation of a planet's or moon's entire solid exterior relative to its spin axis in response to changes in its moment of inertia associated with mass redistribution (*1*). Two first-order controls have been proposed to dictate Earth's TPW rate in geological time: the magnitude of internal inertia perturbations, particularly convective loading that scales with the vigor of mantle convection, and the viscosity of the lower mantle, which is temperature-dependent (*2–5*). These two properties coevolve over Earth's history and are modulated by the secular cooling of the mantle, through which decreasing mantle temperature leads to less vigorous convection and higher viscosity, which should limit rapid TPW (*2–5*).

Paleomagnetic data constrain TPW to ≤3° million year^{-1} (Myr^{-1}) during the Phanerozoic (ca. 539 million years ago [Ma] to present) (*6–9*). More rapid TPW (>4° Myr^{-1}) has been revealed mostly from Neoproterozoic rock records (1,000–539 Ma) (*10–15*). For example, the hypothesized ca. 810–795 Ma Bitter Springs TPW based on paleomagnetic results from the Akademikerbreen Group in Svalbard implied ~83° of cumulative continental motion in ~15 Myr (*10*). However, without direct dates on paleomagnetic poles, uncertainty has lingered in the inferred TPW rates (*10–12*). Similarly, the significance of ca. 850–800 Ma pole motions of Baltica (~90°) remains unresolved without more precise age constraints (*16*, *17*). Moreover, discerning rapid TPW events depends on the geocentric axial dipole (GAD) hypothesis, and large Ediacaran pole shifts have been alternatively speculated to reflect the component of non-GAD fields (*18*, *19*). Lastly, determining the pure TPW signal involves removing simultaneous tectonic movements from the composite pole shift that comprises the two, which has been a longstanding issue of concern to circumvent (*20*).

To estimate TPW rates from the pole shifts complicated by tectonic movements, which remain largely uncertain in the Neoproterozoic, new paleomagnetic poles with records of uniformitarian geomagnetic fields and tight geochronologic controls are required. With precise age determinations of a pole pair, tectonic movements during the time interval can be modeled and subtracted to quantify the pure TPW signal. We have acquired high-precision U-Pb chemical abrasion thermal-ionization mass-spectrometry (CA-TIMS) zircon dates coupled with paleomagnetic poles from Neoproterozoic mafic sills, which intruded in the lower Fanjingshan Group (Gp), Guizhou province, South China. Integrated with existing global data, our new results discover an exceptionally rapid TPW event (>5° Myr^{-1} based on the best estimation) between 832 and 821 Ma, leading to further analysis of the global paleomagnetic database to explore the mechanisms for the changing TPW rate in Earth's history. Our analysis suggests a geodynamic linkage that relates the observed overall decrease and periodic fluctuations in TPW rates with mantle cooling and alternating thermal structures across supercontinent cycles. The resolved geodynamic coupling provides new arrays of predictions for Earth's thermal history and implications for the co-evolution of Earth's interior systems and rotational stability.

Results

The Fanjingshan mafic sills experienced sub-greenschist-grade metamorphism and were folded in the Jiangnan Orogeny (ca. 830–815 Ma) (*21*, *22*), permitting regional fold tests for the paleomagnetic results. We sampled oriented paleomagnetic cores from a total of twelve diabase sills in five sections, with intruded host-rock samples from the Jinzhanping section for a baked contact test (fig. S1). The intrusive contacts of the sampled sills are parallel to bedding (fig. S1,

fig. S2). Five zircon crystals were selected from a geochronologic sample, TS01C, collected from a gabbro-diabase sill for CA-TIMS analysis (fig. S1).

Geochronology

Zircon grains selected for CA-TIMS analysis were euhedral, elongated, similar-sized (~200–300 μm) and with sharp terminations, interpreted to represent crystallization from the same magma. Isotope and age results are reported in Table S1. $^{206}Pb/^{238}U$ versus $^{207}Pb/^{235}U$ ratios show concordant and coherent results (fig. S3A), indicating successful removal of potential lead loss in zircon grains after annealing and chemical abrasion procedures. The weighted mean $^{206}Pb/^{238}U$ date calculated from the zircon analyses gives 831.51 ± 0.32 Ma (2σ uncertainty) (fig. S3, Table S1), representing the crystallization age of the mafic sill.

Paleomagnetism

Seven sills from which 125 specimens were sampled yielded stable and consistent high-temperature components. Two low-temperature components, LT1 and LT2, were first removed during thermal demagnetization. LT1, separated mostly below ~450 °C, is present in most samples and identified as a viscous remanent magnetization (VRM) of the recent geomagnetic field (fig. S5, fig. S6). LT2 (300–350 °C), a southeast-up direction in geographic coordinates, is only found from the five sills in the Huguosi and Jingzhanping sections (fig. S5, fig. S6). LT2 fails a fold test and is also secondary (fig. S6), but its age and origin are relatively unconstrained.

A stable high-temperature component, HT1, carried by magnetite, is identified from all seven sills (~500–580 °C) and their baked contacts (~480–550 °C) (fig. S5). HT1 passes the McFadden fold test (*23*) at 95% confidence level and a progressive unfolding test (*24*) that shows the tightest distribution obtained at 98.9% unfolding (fig. S7), suggesting a magnetization acquired before the folding of the Fanjingshan Gp by ca. 815 Ma (*12*). Paleomagnetic results from the intruded host-rocks in the Jinzhanping section demonstrate a positive baked contact test: baked siltstones record a similar HT1 from that of the sills, while unbaked siltstones preserve a distinct high-temperature component (HT2) from HT1 and other directions determined in the region (fig. S9). The positive baked contact test and fold tests indicate that HT1 is a primary magnetization acquired during the cooling of the sills at 831.51 ± 0.32 Ma.

The corresponding paleomagnetic pole of HT1 (the Fanjingshan pole, 34.7°S, 118.2°E, A_{95} = 8.6) does not resemble any younger pole reported from South China, further supporting a primary origin (Fig.1A, fig. S11). Multiple dispersion parameters of virtual geomagnetic poles (VGPs) fall within expected values of paleosecular variation models (*25*, *26*) (fig. S11), supporting that the Fanjingshan pole has sufficiently recorded the time-averaged position of the geomagnetic pole at ca. 832 Ma, during which the fidelity of the GAD field is also independently substantiated by magnetostratigraphic studies of coeval sedimentary successions (*17*) and comprehensive analyses of the Precambrian geomagnetic field (e.g., *27*).

Discussion

Discovery of rapid TPW between 832 and 821 Ma

The new Fanjingshan pole places the sampling location at a paleolatitude of ~27° at ca. 832 Ma (Fig. 1A). The Fanjingshan pole and the 821.64 ± 0.2 Ma Xiaofeng dykes pole (*28, 29*) quantify the paleolatitudinal displacement of South China to ~41° between 832 and 821 Ma, at an average rate of ≥46.5 ± 15.7 cm yr^{-1} (Fig. 1A). Observational and theoretical speed limits of modern plates

are ~19 cm yr^{-1} and ~20 cm yr^{-1}, respectively (*30*, *31*). The mean latitudinal plate velocity implied by the Fanjingshan and Xiaofeng poles is at least twice the upper limits of the known plate-tectonic speeds. It is thus interpreted to record a combined signal of tectonic movements and TPW. The total pole shift between 832 and 821 Ma is quantified to be 54.7 ± 13.9° with a mean rate of 5.5 ± 1.4° Myr^{-1}.

South China was either disconnected entirely from Rodinia (*12*, *32*, *33*) or located at its periphery during the Tonian (1,000–720 Ma) (*34*). The direction and speed of the tectonic motions of South China between 832 and 821 Ma are currently unknown, due to a paucity of exactly coeval data from other continents for comparison of relative tectonic motion. Considering that signals of TPW and tectonic motion might enhance or counteract each other (*20*), implementing a Monte Carlo method, we simulate tectonic motions of South China between 832 and 821 Ma, by which the total pole shifts are corrected for to constrain quantitatively the pure TPW component (Fig. 2, fig. S15) (Materials and Methods). The disentangled 832–821 Ma TPW rate has an estimated 95% confidence interval of 3.5–7.8° Myr^{-1} (Fig. 2C). The rate is comparable to the hypothesized Bitter Springs TPW constrained to be ≥3.6–4.9° Myr^{-1} for the entire Bitter Springs Stage (from ca. 810 to <795 Ma) (*10*, *11*) and ≥5.4° Myr^{-1} for the first portion of the TPW oscillation (ca. 810–795 Ma) (*12*).

Large paleolatitudinal continental motions during the Tonian were also revealed from the paleomagnetic poles of Baltica (*16*, *17*, *35, 36*). These poles, dated roughly between 850 and 800 Ma, demonstrate a total rotation of ~90°. The pole comparison is illustrated in Fig. 1 C–D, which shows the lining up of the apparent polar wander paths (APWPs) of South China and Baltica between ca. 850 and 810 Ma, reconstructed in relative configurations consistent with those proposed for Rodinia (Euler rotation parameters and references see Table S7). This ca. 850–810 Ma Rodinia APWP is further supported by the ca. 850 Ma Manso dykes pole from West Africa (*37*) and the ca. 820–810 Ma lower Grusdievbreen Formation pole from East Svalbard (*10*), which both fall closely along the APWP defined by the South China and Baltica poles (Fig. 1 C–D). Both East Svalbard and Baltica are considered part of assembled Rodinia in the Tonian (*10*, *36*). The discovery of comparable prominent paleogeographic shifts of congruent Rodinia and presumably separate South China supports the hypothesis that these movements record an extended period of rapid TPW from 850 to 795 Ma: 850–820 Ma equator-ward migration of Rodinia and its associated geoid high ('type I' TPW) (Fig. 1 C–D) followed by 810–795 Ma oscillatory motions about the center of Rodinia (inertial interchange [II] TPW) once the positive geoid docked and stabilized in the equatorial zone (*3*, *5*, *20*, *38*, *39*). Similar to Rodinia, Pangaea was proposed to have witnessed a similar fashion of TPW succession from northward migration (400–250 Ma, I TPW) to equator-centered oscillations (250–100 Ma, II TPW) while at lower average rates (*3*, *39*) (Fig. 3A).

Secular change of TPW over the past billion years

The findings of 850–795 Ma rapid TPW events enable contextualizing the Tonian observations in the evolution of TPW over time. The inferred high Tonian TPW rates exceed the speed limit of observed TPW through the Phanerozoic (~3° Myr^{-1}) (*6–9*) and theoretical constraints (~2.4° Myr^{-1}) (*2*) with present-day lower mantle viscosity estimates. Numerical simulations suggest that rapid TPW at >4° Myr^{-1} with a max rate of ~6° Myr^{-1} can be achieved with substantially increased convective flow (*4*) and/or reduced lower mantle viscosity to ~3–10 10^{21} Pa s, 10–30% of the present value (*3*) consistent with thermal history modeling for the Tonian (*40*). These comparisons support a more vigorously convecting and less viscous mantle in the Tonian that

allowed more rapid reorganization between principal moments of inertia. We synthesize and analyze the extant probable estimates for the TPW rate over the past billion years (Fig. 3A, Table S8). The time series manifests a general decreasing nature of the rate since the Tonian, a significant drop toward the Cambrian (from 832 to 505 Ma), and a relatively more stable state through the Phanerozoic (505–0 Ma) (Fig. 3A). Two TPW peaks occur at around 832–795 Ma and 170–80 Ma, coinciding with the early breakup of Rodinia and Pangaea, respectively (*41*, *42*). The Ediacaran rapid polar wander rates (conservative estimates) appear to be compatible with an implied TPW reduction from the Tonian to the early Phanerozoic if TPW rather than non-GAD fields was the driving mechanism (Fig. 3A) (*13*, *15*).

We propose a geodynamic link to explain both the systematic decrease in the TPW rate and episodic variations imposed over the mean trend since the late Mesoproterozoic, in which mantle cooling coupled with supercontinent cycles. The observed overall secular TPW decline is consistent with TPW rate controlled primarily by increasing lower mantle viscosity and declining vigor of mantle convection as Earth's interior cooled (*3–5*) (Fig. 3A, fig. S14). The two high TPW stages, between 832–795 Ma and 170–80 Ma (Fig. 3A), coincide with transitions in the Rodinia and Pangaea supercontinent cycles: preceded by protracted supercontinent thermal insulation and succeeded shortly by supercontinent dispersal (*42–44*). During the 1800–850 Ma Nuna-Rodinia lifetime (*44, 45*) and the 320–180 Ma Pangaea lifetime (*7*), supercontinents rimmed by peripheral subduction zones may have partially insulated the underlying mantle and altered mantle thermal structures: warming the subcontinental mantle and cooling the suboceanic mantle (temperature variation on the order of 100 °C or greater) (*46–48*). This insulating regime resulted in inhibited convective mixing between the subcontinental and suboceanic domains, localized mantle flow patterns relative to the supercontinent, raised viscosity of voluminous suboceanic mantle, and associated decreased velocity of oceanic plates (*46, 47*), setting the stage for slow TPW (Fig. 3A–B). The 1,110–1,080 Ma TPW rates appear to have been restrained more considerably – a presumed consequence of longer-lived insulation by Nuna and Rodinia compared to Pangaea, creating greater lateral mantle thermal and viscosity variations (*46*, *47*).

As heat accumulated beneath the subcontinental region and the lateral hydrostatic pressure gradient built up in the mantle, the peripheral subduction girdle was destabilized and a supercontinent approached the wake of dispersal (*39*, *46–48*). Breakdown of a subduction girdle would re-establish large-scale advective exchange between the subcontinental and suboceanic mantle, relaxing mantle thermal and viscosity anomalies (*46*). This mantle thermal mixing involves unleashing a pulse of increased convective vigor driven by the preexisting lateral temperature gradient, accelerated overturn of oceanic plates, and enhanced global convective motions (*45–48*), invigorating mass redistributions in Earth's interior and on the surface that speed up TPW. Meanwhile, as mantle thermal re-equilibrium proceeds, warming the once cooled and more viscous suboceanic mantle might reduce the maximum viscosity of the lower mantle (rate-limiting TPW), which potentially relaxes the restriction on TPW rates (*5*). Such a changeover of mantle thermal state could take over ~100 Myr to accomplish (*46–48*) and may explain the accelerated TPW rates prompted at 832–795 Ma, 170–145 Ma, and ca. 80 Ma, succeeding the breakup of Rodinia and Pangaea (Fig. 3). Following supercontinent breakup, elevated mantle flow, surface heat flux, and lithospheric mobility would have amplified mantle cooling rates initially, followed by gradual restoration to baseline cooling trend as convective forcing weakens toward the completion of mantle thermal mixing (*46–48*). The relaxed convective vigor contributes to the subsequent decline and stabilization of TPW rates until the formation of the next supercontinent cycle (Fig. 3A). This model, if valid, underscores the

increasing importance of accounting for large-scale and varying lateral thermal heterogeneities associated with mantle thermal structures in future numerical modeling of TPW.

Notably, the striking reduction in TPW rate during the Neoproterozoic might suggest an irreversible transition, after which the mantle cooled enough to render a slow-TPW regime in the Phanerozoic (<3° Myr^{-1}), also characterized by an overall smaller amplitude of variation in TPW rates (Fig. 3A). This implied mantle thermal decline in the Neoproterozoic resonates with coeval lithospheric evidence showing a rising dominance of low thermobaric ratios (*T*/*P*) of rock records since the Tonian that subsequently persisted through the Phanerozoic (*44*, *49*). The promoted and continual prevalence of low *T*/*P* metamorphic records, i.e., the blueschist-facies and ultrahigh-pressure metamorphism, is inferred to be directly linked to cooling of the upper mantle, leading to colder, denser, and strengthened oceanic lithosphere and deeper slab breakoff in the collision zones (*49*, *50*). Numerical models suggest such a transition in the style of orogenesis from hotter to colder may have taken place as the mantle temperature fell to ~80–100 °C higher than present-day values (*50*), corresponding to an inferred Neoproterozoic timing constrained by igneous rock records and thermal modeling (*51*). Such mantle heat loss may have been facilitated by plate-tectonic activity since the Tonian associated with the breakup of Rodinia (peaking at ca. 800–600 Ma) and the assembly of Gondwana (ca. 650–500 Ma) (*52*). In particular, cooling may have been facilitated by extensive circum-supercontinent subduction zones and internal rifting (*52*). Consequently, by the early Cambrian, progressively reduced mantle heat, which would have led to suppressed mantle convection and raised viscosity, in turn, deactivated mantle physical conditions favorable for prompting rapid TPW in succeeding periods (Fig. 3A).

Characterizing the secular change of TPW raises further opportunities and considerations in paleogeographic reconstructions. The established framework provides testable predictions for facilitating subsequent explorations of TPW to improve and revise our extant understanding. Despite an expanding global TPW database, records of well-defined TPW excursions have remained generally elusive. Nevertheless, the importance of high-resolution sampling in resolving fast while smaller-amplitude TPW (~10°) has been demonstrated recently (*9*), which suggests more potential missing TPW signals to search for, especially during the dynamic TPW stages as our model predicts (Fig. 3). With better characterization of TPW from new observations, full accounting of TPW motions, including periods throughout supercontinent transitions, may become available to aid in the solution of absolute paleolongitude of ancient plates (*53*). The secular change of TPW also gives insights into tracing the changing rate of plate tectonics. As TPW manifests with coherent motion of global plates, the intervals of large-scale TPW would reinforce the sensitivity in quantifying plate-tectonic rates concurrently with TPW, as already explored by analyzing differences of contemporaneous pole motions (e.g., *12*, *54*). Most existing estimates of Proterozoic plate velocities are not corrected for possible TPW (e.g., *55*), particularly for the Neoproterozoic when TPW was likely faster and more variable. Discerning rates between TPW and tectonic movement in Earth's deep time would enable probing possible coupling of the two in the long term, both functions of evolving mantle thermal history and cyclic transformations in continental configurations and mantle structures (*1*, *3–5*, *31*, *46*).

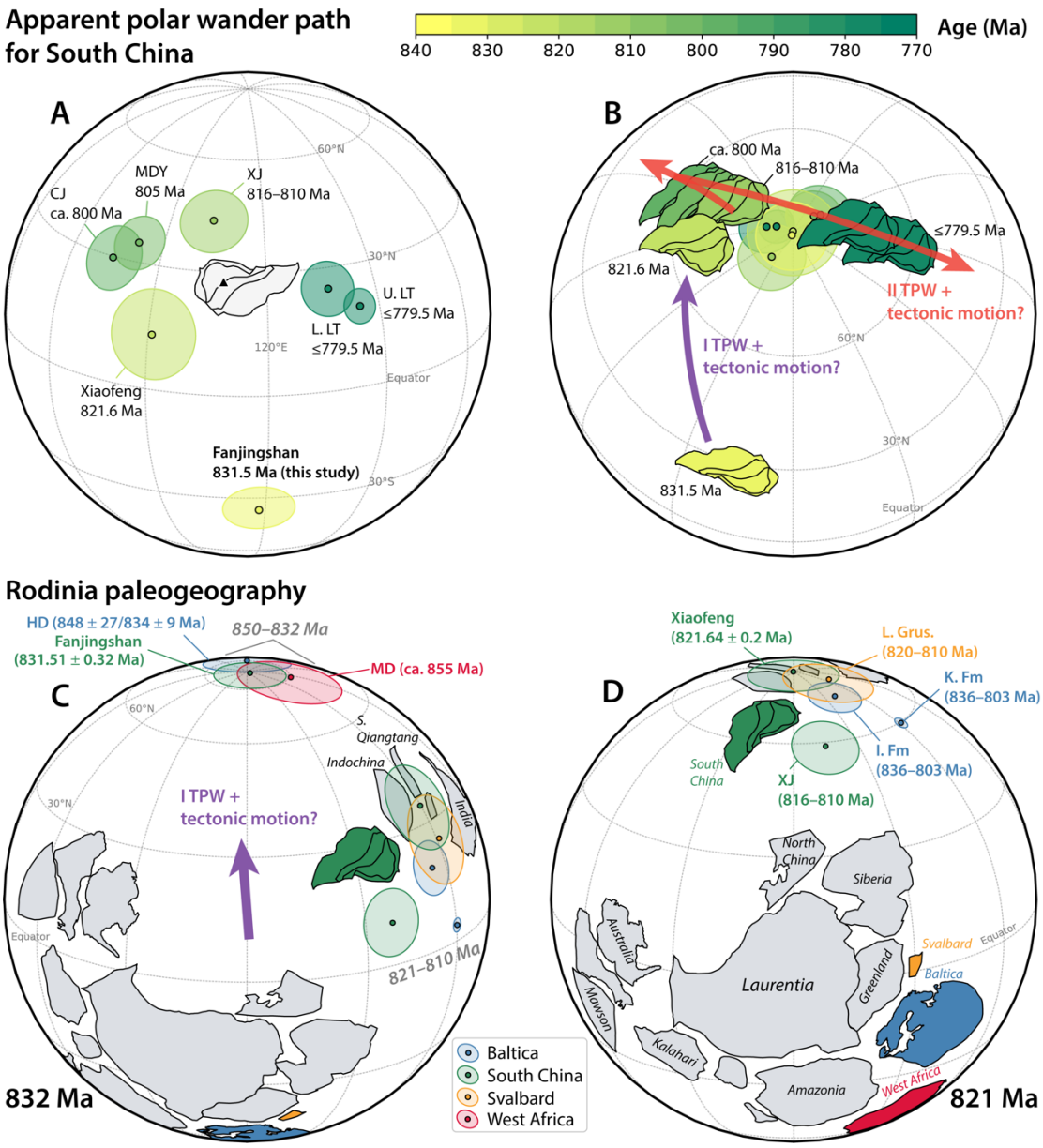

Figure 1. Mid-Tonian paleogeographic models for South China and Rodinia. (**A**) Tonian apparent polar wander path (APWP) of South China. Ellipses show A_{95}, the 95% confidence cones of the poles. Triangle signifies the mean sampling locality of the Fanjingshan sills (27.92°N, 108.69°E) for paleolatitude conversion. See Table S3 for details of data. (**B**) The proposed paleogeographic model for South China reconstructed with the APWP in (A). Paleogeographic changes between 816 and 780 Ma follow the preferred 'minimize difference' model from (*12*). Hybrid TPW + tectonic motions are interpreted for 832–821 Ma and 816–795 Ma. (**C** and **D**) Rodinia paleogeographic changes in the context of 832–821 Ma 'type I' TPW. Poles and Euler rotation parameters are provided in Table S3 & S4 & S7. Pole abbreviations: CJ—Chengjiang Formation; MDY—Madiyi Formation; XJ—Xiajiang Group; L. LT—lower Liantuo Formation; U. LT—upper Liantuo Formation; HD—Hunnedalen dykes; MD—Manso dykes; L. Grus.—lower Grusdievbreen Formation; K. Fm—Katav Formation; I. Fm—Inzer Formation.

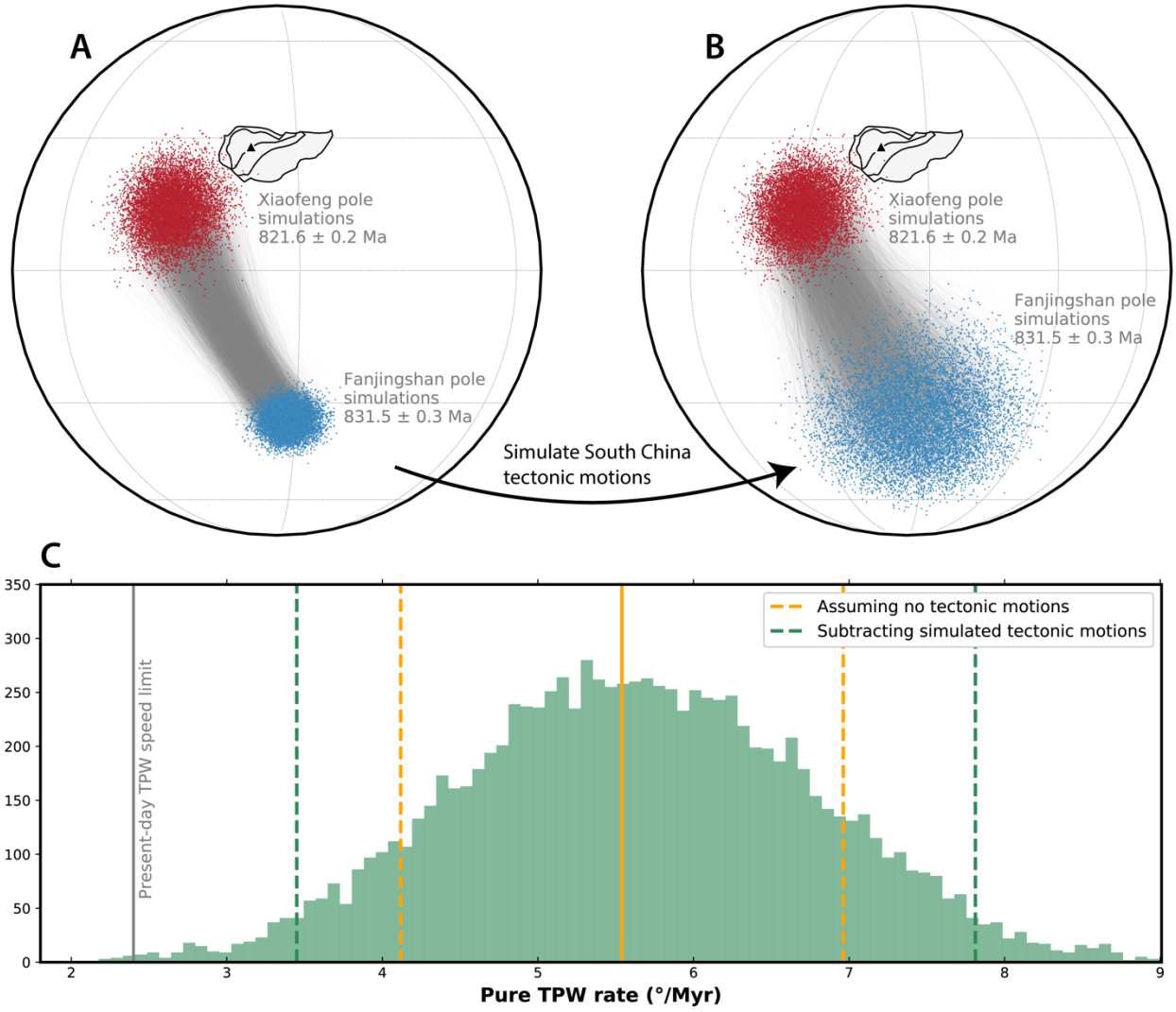

Figure 2. 832–821 Ma TPW rate estimated using Monte Carlo analysis. (**A**) Resampled Fanjingshan and Xiaofeng poles from Fisher distribution (n = 10,000 for each). Pole pairs are randomly drawn between the two pole groups, connected with fine grey lines representing angular distance. Triangle indicates the mean sampling locality of the Fanjingshan sills (27.92°N, 108.69°E). (**B**) Simulation of South China tectonic motions between 832 and 821 Ma assuming a speed limit of implied fastest Neoproterozoic plate-tectonic velocities (~31 cm yr^{-1}) (*56*) with unconstrained directions and application of these displacements to the resampled Fanjingshan poles from (A). The resultant new pole pairs reflect the pure TPW component after subtracting simulated tectonic motions. Dividing the pure TPW angular distances by the age differences between the pole pairs yields pure TPW rate estimates. (**C**) Histogram of pure TPW rate estimates from (B). The green dashed lines bound the 95% confidence intervals of the TPW rate after accounting for simulated tectonic motions (3.5–7.8° Myr^{-1}). The orange solid and dashed lines show the mean rate and 2σ uncertainties of the total pole shift between the Fanjingshan and Xiaofeng poles using standard error propagation (5.5 ± 1.4° Myr^{-1}) (Materials and Method), which could reflect TPW estimates only when assuming no tectonic motions of South China. The grey solid line shows the proposed TPW speed limit (~2.4° Myr^{-1}) set by present-day mantle viscosity estimates (*2*). See Materials and Methods for details.

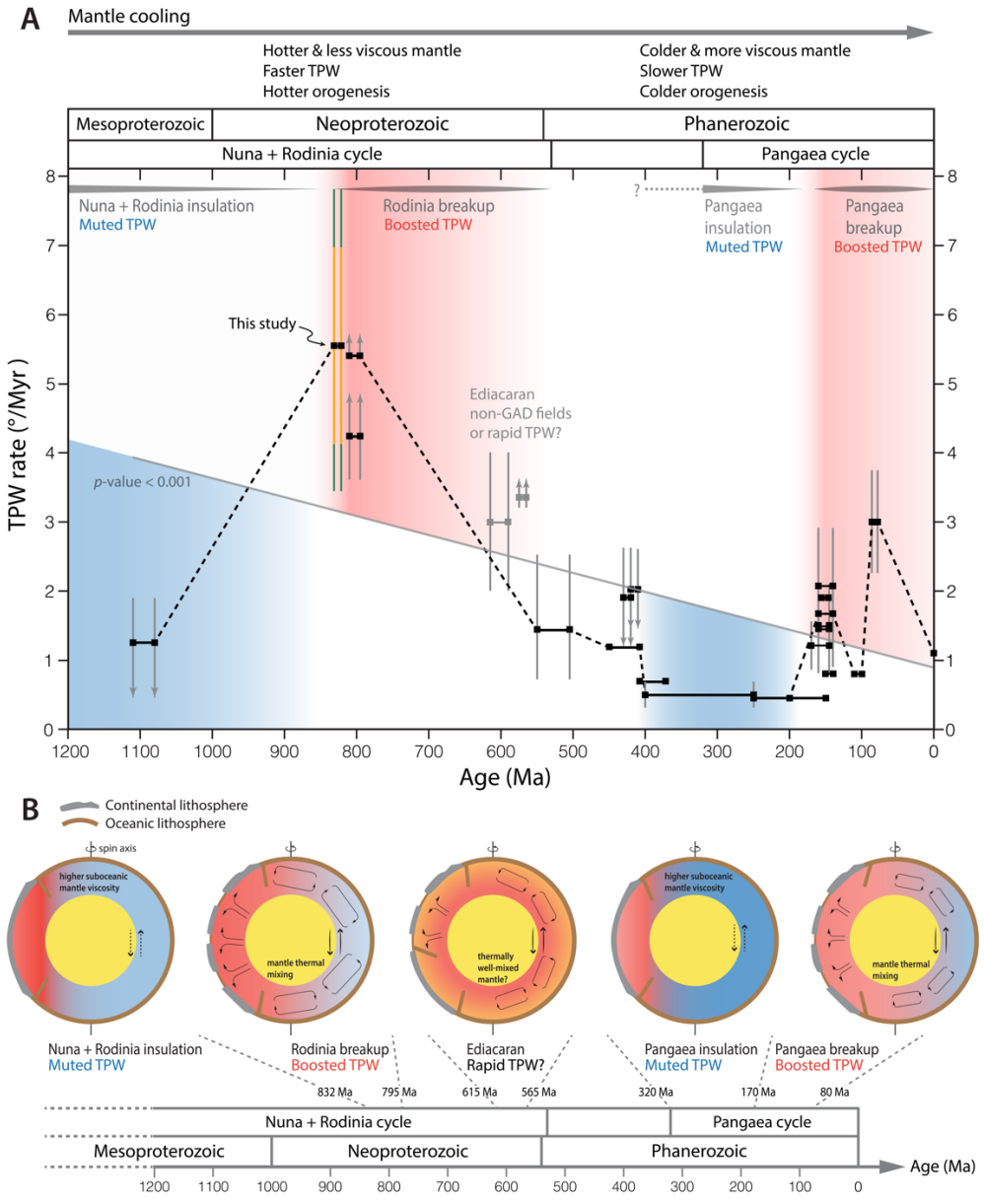

Figure 3. Secular change of the TPW rate and our proposed geodynamic coupling. (**A**) Probable TPW rate estimates since the late Mesoproterozoic. TPW rates and uncertainties are summarized in Supplementary Text and tabulated in Table S8. The grey solid line indicates a linear regression fit of the data (p-value < 0.001) that characterizes the first-order decreasing trend (the fit excludes the Ediacaran data of debated origins, shown as grey squares). See fig. S14 for sensitivity tests that also consider variously interpreted Ediacaran TPW rate estimates. The black dashed line traces the second-order variation in TPW connected by representative rate estimates of individual time intervals. Grey vertical bars show the uncertainties of rate estimates. Up/down arrows indicate that the rate could be above/below the shown range defined by the error bars. For the TPW rate uncertainty of this study, the orange bar represents considering no tectonic motions and the green bar reflects accounting for simulated tectonic motions (corresponding to those shown in Fig. 2C). (**B**) Schematic illustration of secular change of TPW related to mantle cooling and alternating mantle thermal structures linked to assembly and breakup of continents (supercontinent aggregation–mantle thermal insulation–muted TPW; supercontinent breakup–mantle thermal mixing–boosted TPW).

Materials and Methods

Field sampling

Paleomagnetic cores were collected using a portable gasoline-powered drill with non-magnetic, diamond-rimmed bites. The intrusive contacts of the sampled mafic sills are parallel to the bedding of the country rocks (sandstone and siltstone of the lower Fanjingshan Group). Sills with clearly observable contacts were prioritized for sampling. The seven sills that yielded stable and consistent high-temperature components used to calculate the pole all have direct bedding controls. Multiple bedding measurements were made for the country rocks closely adjacent to the contacts to calculate the mean bedding for each sill (Table S2). The thickness of the sampled sills is typically over ten meters. Each sill was drilled evenly across its thickness to average the characteristic remanent magnetization. Where measured close to the sampling sites, no significant bedding difference was observed for the upper and lower contacts of each sill, indicating a consistent emplacement of each sill along bedding at each of the sampling localities. Therefore, we adopt a common mean bedding for samples collected from the same sill. We measured the orientation of the cores in the field using a combination of the magnetic compass and sun compass when the sun was available. No significant difference is observed between the two orientation methods.

U-Pb geochronology

Zircon separation from block samples was performed at Harvard University using standard techniques. Zircon U-Pb geochronology was conducted in the Isotope Laboratory at NERC Isotope Geoscience Laboratories (NIGL) at British Geological Survey. Separated zircon crystals were annealed in a muffle furnace at 900 °C for 60 hours in quartz beakers. Selected zircon grains were transferred to 3 ml Hex Savillex beakers. They were processed through ultrasonic bathing and rinsing with 30% HNO_3 and then moved to 300 µl Teflon PFA micro-capsules to be leached in an about 5:1 mix of 29 M HF and 30% HNO_3 for 12 hours at 180 °C. After removing the leachate, the residues were rinsed again with 30% HNO_3 and 6 M HCl and spiked with the EARTHTIME ^{235}U–^{233}U–^{205}Pb tracer (*57*). Each zircon grain was then fully dissolved in about 120 µl of 29M HF with a trace amount of 30% HNO_3 at 220 °C for 48 hours. The solutions were then dried, and fluorites in the samples were converted to chlorides in 3 M HCl at about 180 °C overnight. Standard HCl-based anion-exchange chromatographic procedures were performed to separate U and Pb from each sample, then loaded on a single Re filament in a silica-gel–phosphoric acid mixture. Isotope ratios of U and Pb were analyzed using the Thermo-Electron Triton TIMS system in NIGL. U isotopes were measured in static Faraday mode or on a single SEM detector, depending on the uranium contents. Pb isotopes were measured using the peak-hopping method with a single SEM detector. Data reductions were processed in Tripoli (*58*). U-Pb concordia diagrams were plotted using IsoplotR (*59*).

Paleomagnetic and rock magnetic experiments

Paleomagnetic and rock magnetic experiments were performed in Paleomagnetism and Environmental Magnetism Laboratory at the China University of Geosciences, Beijing. Oriented paleomagnetic cores were first sliced into cylindrical specimens of ~1–2.2 cm thickness using non-magnetic, diamond-rimmed saw blades. Remanent magnetizations of all specimens were measured with a 2G 755-4 K three-axis cryogenic magnetometer in a magnetic shield room with a <300 nT residual field. Specimens were processed through stepwise thermal demagnetization in either an ASC TD-48 or MMTDSC furnace that holds an internal residual field of <10 nT. Most

specimens were completely demagnetized in ~20–35 steps by up to ~580 °C. Temperature increment between each step varies between 20–40 °C in the low-temperature range (<500 °C) and 3–10 °C in the high-temperature range (500–580 °C). Some specimens were subject to small demagnetizing increments of 5–10 °C between 300–350 °C to characterize better the removal of low-temperature components in this interval. To identify the carriers of magnetic remanences, temperature-dependent low field susceptibility of representative samples (ground to fine powders) was measured in an argon atmosphere with an AGICO KLY-4S Kappabridge with CS-3 high-temperature device. Heating and cooling curves were acquired between room temperature and 700 °C.

Paleomagnetic analyses and calculations

Remanence components were fit using linear principal component analysis (*60*). Unless specified, we force the best-fit lines to pass through the origin when fitting the high-temperature components. Only specimens with ≥4 stable points that decay to the origin with MAD (maximum angle of deviation) smaller than 20° in the high-temperature interval are regarded as credible and used to calculate specimen directions. Specimen directions were then averaged using Fisher statistics (*61*) to calculate the site mean direction of each sill/site of sedimentary rocks. Specimen analysis was done using the Paleomag OS X program (*62*). Paleomagnetic analyses and plotting were completed in Python facilitated by the PmagPy package (*63*).

To quantify the rate of pole shift between a pair of poles, we incorporate full error propagation in the calculation considering uncertainties in both the ages and positions of the poles. Given the great-circle distance [$\Delta\theta$ (°)] and age difference [Δt (Myr)] between two poles, *a* and *b*, the mean rate of pole shift (° Myr^{-1}) with 2σ error is calculated as follows:

$$rate = \frac{\Delta\theta}{\Delta t}\left(1 \pm \sqrt{\frac{\sigma_{(a)}{}^2+\sigma_{(b)}{}^2}{(\Delta t)^2} + \frac{A_{95(a)}{}^2+A_{95(b)}{}^2}{(\Delta\theta)^2}}\right) \quad (1)$$

Where A_{95} is the radius of the 95% confidence cone of the pole; σ is the 2σ uncertainty on the pole age.

We take a Monte Carlo approach to further constrain the range of pure TPW rates between 832 and 821 Ma inferred from the Fanjingshan and Xiaofeng poles. From Fisher distributions, a large number (10,000) of random virtual geomagnetic poles (VGPs) are simulated for each paleomagnetic pole according to their pole positions and associated uncertainties (Table S3), paired with random draws from Gaussian distributions for the pole ages (831.51 ± 0.32 Ma and 821.64 ± 0.2 Ma). Simulated VGPs from each pole group are paired randomly, connected by grey arcs shown in Fig. 2A.

To account for the potential pole shift produced by tectonic movement and disentangle the pure TPW component, we simulate tectonic movements of South China between 832–821 Ma and subtract them from the total pole motion. The direction and velocity of tectonic movements of South China during this period are currently unclear. As such, for simulating the tectonic speed, we adopt a triangular distribution (fig. S15) assuming:

1. The lower speed limit at 0 cm yr^{-1}.
2. The mode at 10 cm yr^{-1} that corresponds to the fastest plate velocity of South China extracted from the Neoproterozoic plate kinematic models by (*55*).

3. The upper speed limit at 31 cm yr^{-1} that represents the possible fastest tectonic movement implied since the late Mesoproterozoic (*56*).

Unconstrained directions of South China tectonic movements are assumed to accommodate the largest effect of tectonic motions. We take 10,000 random draws from the tectonic speed distribution described above (fig. 15), and directions of the tectonic motions are randomly sampled from 0–360° from uniform distributions. These simulated tectonic speeds paired with random directions are multiplied by the simulated age differences to obtain the distances of tectonic movements between 832 and 821 Ma. The series of tectonic movements are then randomly applied to the sampled Fanjingshan poles in Fig. 2A to convert the effect of plate motions to its paleomagnetic expression. Fig. 2B shows the displaced Fanjingshan poles after correcting for simulated tectonic motions, leaving the new angular difference between each pole pair an estimate of the pure TPW component. Finally, the pure TPW angular distance is divided by the age difference between the pole pair to estimate the pure TPW rate (Fig. 2C). The 2.5 and 97.5 percentiles are taken from the rate distribution, interpreted as the 95% confidence intervals (Fig. 2C). Accounting for tectonic motions yields a larger spectrum of TPW rate estimations compared with assuming zero plate displacement (Fig. 2C). The expanded upper tail corresponds to scenarios where the total pole motion is produced by TPW counteracted by tectonic motion, resembling the case interpreted for South China between 815 and 800 Ma (*12*) and North China in the late Jurassic (*54*). Whereas the reduced lower tail corresponds to TPW and tectonic motion moving along similar directions and acting additively, similar to the interpretation for Laurentia between ca. 1,110 and 1,080 Ma (*56*).

References and Notes:

1. I. Matsuyama, F. Nimmo, J. X. Mitrovica, Planetary reorientation. *Annu. Rev. Earth Planet. Sci* **42**, 605–634 (2014).
2. V. Tsai, D. Stevenson, Theoretical constraints on true polar wander. *J. Geophys. Res. Solid Earth* **112**, (2007).
3. J. R. Creveling, J. X. Mitrovica, N.-H. Chan, K. Latychev, I. Matsuyama, Mechanisms for oscillatory true polar wander. *Nature* **491**, 244–248 (2012).
4. I. Rose, B. Buffett, Scaling rates of true polar wander in convecting planets and moons. *Phys. Earth Planet. Inter.* **273**, 1–10 (2017).
5. T. D. Raub, J. L. Kirschvink, D. A. D. Evans, True Polar Wander: Linking Deep and Shallow Geodynamics to Hydro- and Biospheric Hypotheses. In *Treatise on Geophysics*, pp. 565–89 (Elsevier, 2007).
6. B. Steinberger, T. Torsvik, Absolute plate motions and true polar wander in the absence of hotspot tracks. *Nature* **452**, 620–623 (2008).
7. T. H. Torsvik, R. Van der Voo, U. Preeden, C. Mac Niocaill, B. Steinberger, P. V. Doubrovine, D. J. J. van Hinsbergen, M. Domeier, C. Gaina, E. Tohver, J. G. Meert, P. J. A., McCausland, L. R. M. Cocks, Phanerozoic polar wander, palaeogeography and dynamics. *Earth-Sci. Rev.* **114**, 325–368 (2012).
8. D. V. Kent, B. A. Kjarsgaard, J. S. Gee, G. Muttoni, L. M. Heaman, Tracking the Late Jurassic apparent (or true) polar shift in U-Pb-dated kimberlites from cratonic North America (Superior Province of Canada). *Geochem. Geophys. Geosyst.* **16**, (2015).
9. R. N. Mitchell, C. J. Thissen, D. A. Evans, S. P. Slotznick, R. Coccioni, T. Yamazaki, J. L. Kirschvink, A Late Cretaceous true polar wander oscillation. *Nat. Commun.* ***12***, 1–8 (2021).

10. A. C. Maloof, G. P. Halverson, J. L. Kirschvink, D. P. Schrag, B. P. Weiss, P. F. Hoffman, Combined paleomagnetic, isotopic, and stratigraphic evidence for true polar wander from the Neoproterozoic Akademikerbreen Group, Svalbard, Norway. *GSA Bulletin* **118**, 1099–1124 (2006).
11. N. L. Swanson-Hysell, A. C. Maloof, D. J. Condon, G. R. T. Jenkin, M. Alene, M. M. Tremblay, T. Tesema, A. D. Rooney, B. Haileab, Stratigraphy and geochronology of the Tambien Group, Ethiopia: evidence for globally synchronous carbon isotope change in the Neoproterozoic. *Geology* **43**, 323–326 (2015).
12. Y. Park, N. L. Swanson-Hysell, H. Xian, S. Zhang, D. J. Condon, H. Fu, F. A. Macdonald, A consistently high-latitude south China from 820 to 780 Ma: Implications for exclusion from Rodinia and the feasibility of large-scale true polar wander. *J. Geophys. Res. Solid Earth* **126**, (2021).
13. R. N. Mitchell, T. M. Kilian, T. D. Raub, D. A. Evans, W. Bleeker, A. C. Maloof, Sutton hotspot: Resolving Ediacaran-Cambrian Tectonics and true polar wander for Laurentia. *Am. J. Sci.* **311 (8)**, 651–663 (2011).
14. B. Robert, J. Besse, O. Blein, M. Greff-Lefftz, T. Baudin, F. Lopes, Constraints on the Ediacaran inertial interchange true polar wander hypothesis: A new paleomagnetic study in Morocco (West African craton). *Precambrian Res*. **295**, 90–116 (2017).
15. B. Robert, M. Greff-Lefftz, J. Besse, True polar wander: A key indicator for plate configuration and mantle convection during the late Neoproterozoic. *Geochem. Geophys. Geosyst.* **19**, 3478–3495 (2018).
16. V. Pavlov, Y. Gallet, Katav limestones: a unique example of remagnetization or an ideal recorder of the Neoproterozoic geomagnetic field? *Izvestiya Phys. Solid Earth* **45**, 31–40 (2009).
17. V. Pavlov, Y. Gallet, Variations in geomagnetic reversal frequency during the Earth's middle age. *Geochem. Geophys. Geosyst.* **11**, (2010).
18. A. Abrajevitch, R. Van der Voo, Incompatible Ediacaran paleomagnetic directions suggest an equatorial geomagnetic dipole hypothesis. *Earth Planet. Sci. Lett.* **293**, 164–170 (2010).
19. R. K. Bono, J. A. Tarduno, A stable Ediacaran Earth recorded by single silicate crystals of the ca. 565 Ma Sept-Îles intrusion: *Geology* **43**, 131–134 (2015).
20. D. A. D. Evans, True polar wander and supercontinents. *Tectonophysics* **362**, 303–320 (2003).
21. J.-C. Zhou, X.-L. Wang, J.-S. Qiu, Geochronology of Neoproterozoic mafic rocks and sandstones from northeastern Guizhou, South China: Coeval arc magmatism and sedimentation. *Precambrian Res.* **170**, 27–42 (2009).
22. J. Yao, P. A. Cawood, L. Shu, G. Zhao, Jiangnan Orogen, South China: A ~970–820 Ma Rodinia margin accretionary belt. *Ear-Sci Rev.* **196**, 102–872 (2019).
23. P. L. McFadden, A new fold test for palaeomagnetic studies. *Geophys. J. Int.* **103**, 163–169 (1990).
24. G. S. Watson, R. J. Enkin, The fold test in paleomagnetism as a parameter estimation problem. *Geophys. Res. Lett.* **20**, 2135–2137 (1993).
25. T. Veikkolainen, L. J. Pesonen, Palaeosecular variation, field reversals and the stability of the geodynamo in the Precambrian. *Geophys. J. Int.* **199**, 1515–1526 (2014).
26. M. H. L. Deenen, C. G. Langereis, D. J. J. van Hinsbergen, A. J. Biggin, Geomagnetic secular variation and the statistics of palaeomagnetic directions. *Geophys. J. Int.* **186**, 509–520 (2011).

27. T. Veikkolainen, L. J. Pesonen, Precambrian geomagnetic field—an overview. In L. J. Pesonen, D. A. D. Evans, S. ˚A. Elming, J. M. Salminen, T. Veikkolainen (Eds.), *Ancient supercontinents and the paleogeography of the earth* (2021).
28. Z.-X. Li, D. A. D. Evans, S. Zhang, A 90° spin on Rodinia: possible causal links between the Neoproterozoic supercontinent, superplume, true polar wander and low- latitude glaciation. *Earth Planet. Sci. Lett.* **220**, 409–421 (2004).
29. T.-T. Wang, S. Zhang, J. Ramezani, Age Recalibration of the Xiaofeng Dykes, South China, and Its Implications for True Polar Wander at ~820 Ma. Acta Geologica Sinica (English Edition) **90**, 47 (2016).
30. D. J. J. van Hinsbergen, B. Steinberger, P. V. Doubrovine, R. Gassmöller, Acceleration and deceleration of India-Asia convergence since the Cretaceous: Roles of mantle plumes and continental collision. *J. Geophys. Res. Solid Earth* **116**, (2011).
31. S. Zahirovic, R. D. Müller, M. Seton, N. Flament, Tectonic speed limits from plate kinematic reconstructions. *Earth Planet. Sci. Lett.* **418**, 40–52 (2015).
32. H. Xian, S. Zhang, H. Li, T. Yang, H. Wu, Geochronological and palaeomagnetic investigation of the Madiyi Formation, lower Banxi Group, South China: Implications for Rodinia reconstruction. *Precambrian Res.* **336**, 105494 (2020).
33. L. Chang, S. Zhang, H. Li, H. Xian, H. Wu, T. Yang, New Paleomagnetic Insights Into the Neoproterozoic Connection Between South China and India and Their Position in Rodinia. *Geophys. Res. Lett.* ***49***, (2022).
34. P. A. Cawood, G. Zhao, J. Yao, W. Wang, Y. Xu, Y. Wang, Reconstructing south China in Phanerozoic and Precambrian supercontinents. *Ear-Sci Rev* **186**, 173–194 (2017).
35. H. J. Walderhaug, T. H. Torsvik, E.A. Eide, B. Sundvoll, B. Bingen, Geochronology and palaeomagnetism of the Hunnendalen dykes, SW Norway: implications for the Sveconorwegian apparent polar wander loop. *Earth Planet. Sci. Lett*. **169**, 71–83 (1999).
36. L. M. Fairchild, N. L. Swanson-Hysell, J. Ramezani, C. J. Sprain, S. A. Bowring, The end of Mid continent Rift magmatism and the paleogeography of Laurentia. *Lithosphere* **9**, 117–133 (2017).
37. P. Y. J., Antonio, L. Baratoux, R. I. F. Trindade, S. Rousse, A. Ayite, C. Lana, M. Macouin, E. W. K. Adu, C. Sanchez, M. A. L. Silva, A. S. Firmin, West Africa in Rodinia: High quality paleomagnetic pole from the~ 860 Ma Manso dyke swarm (Ghana). *Gondwana Res.* **94**, 28–43 (2021).
38. S. Zhong, N. Zhang, Z. X. Li, J. H. Roberts, Supercontinent cycles, true polar wander, and very long wave-length mantle convection. *Earth Planet. Sci. Lett.* **261**, 551–564 (2007).
39. X. Le Pichon, M. Jellinek, A. Lenardic, A. M. C. Şengör, C. İmren, Pangea Migration. *Tectonics* **40***,* (2021).
40. J. W. Crowley, M. Gérault, R. J. O'Connell, On the relative influence of heat and water transport on planetary dynamics. *Earth Planet. Sci. Lett.* **310**, 380–388 (2011).
41. Z. X. Li, S. V. Bogdanova, A. S. Collins, A. Davidson, B. De Waele, R. E. Ernst, et al., Assembly, configuration, and break-up history of Rodinia: A synthesis. *Precambrian Research* **160**, 179–210 (2008).
42. H. Van Avendonk, J. Davis, J. Harding, Decrease in oceanic crustal thickness since the breakup of Pangaea. *Nat. Geosci.* **10,** 58–61 (2017).
43. P. A. Brandl, M. Regelous, C. Beier, K. M. Haase, High mantle temperatures following rifting caused by continental insulation. *Nat. Geosci.* **6**, 391–394 (2013).

482 44. M. Brown, C. L. Kirkland, T. E. Johnson, Evolution of geodynamics since the Archean:
483 Significant change at the dawn of the Phanerozoic. *Geology* **48**, 488–492 (2020).
484 45. M. Tang, X. Chu, J. Hao, B. Shen, Orogenic quiescence in Earth's middle age. *Science* **371**,
485 728–731 (2021).
486 46. A. Lenardic, L. Moresi, A. M. Jellinek, C. J. O'Neill, C. M. Cooper, C. T. Lee, Continents,
487 supercontinents, mantle thermal mixing, and mantle thermal isolation: Theory, numerical
488 simulations, and laboratory experiments, *Geochem. Geophys. Geosyst.* **12**, (2011).
489 47. A. M. Jellinek, A. Lenardic, R. T. Pierrehumbert, Ice, Fire, or Fizzle: The Climate Footprint
490 of Earth's Supercontinental Cycles. *Geochem. Geophys. Geosyst.* **21**, (2020).
491 48. A. Lenardic, A supercontinental boost. *Nat. Geosci.* **10**, 4–5 (2017).
492 49. R. J. Stern, The evolution of plate tectonics. *Philos. Trans. Royal Soc.* **A376**, 20170406
493 (2018).
494 50. E. Sizova, T. Gerya, M. Brown, Contrasting styles of Phanerozoic and Precambrian
495 continental collision. *Gondwana Res.* **25**, 522–545 (2014).
496 51. C. Herzberg, K. Condie, J. Korenaga, Thermal history of the Earth and its petrological
497 expression. *Earth Planet. Sci. Lett.* **292**, 79–88 (2010).
498 52. P. A. Cawood, R. A. Strachan, S. A. Pisarevsky, D. P. Gladkochub, J. B. Murphy, Linking
499 collisional and accretionary orogens during Rodinia assembly and breakup: implications for
500 models of supercontinent cycles. *Earth Planet. Sci. Lett.* **449**, 118–126 (2016).
501 53. R. N. Mitchell, T. M. Kilian, D. A. Evans, Supercontinent cycles and the calculation of
502 absolute palaeolongitude in deep time. *Nature **482***, 208–211 (2012).
503 54. Y. Gao, S. Zhang, H. Zhao, Q. Ren, T. Yang, H. Wu, H. Li, North China block underwent
504 simultaneous true polar wander and tectonic convergence in late Jurassic: New
505 paleomagnetic constraints. *Earth Planet. Sci. Lett.*, **567**, 117012 (2021).
506 55. A. S. Merdith, A. S. Collins, S. E. Williams, S. Pisarevsky, J. D. Foden, D. B. Archibald, M.
507 L. Blades, B. L. Alessio, S. Armistead, D. Plavsa, C. Clark, R. D. Müller, A full-plate global
508 reconstruction of the Neoproterozoic. *Gondwana Res.* **50**, 84–134 (2017).
509 56. N. L. Swanson-Hysell, J. Ramezani, L. M. Fairchild, I. R. Rose, Failed rifting and fast
510 drifting: Mid-continent Rift development, Laurentia's rapid motion and the driver of
511 Grenvillian orogenesis. *GSA Bulletin* **131**, 913–940 (2019).
512 57. D. J. Condon, B. Schoene, N. M. McLean, S. A. Bowring, R. R. Parrish, Metrology and
513 traceability of U–Pb isotope dilution geochronology (EARTHTIME Tracer Calibration Part
514 I). *Geochim. Cosmochim. Acta* **164**, 464–480 (2015).
515 58. J. F. Bowring, N. M. McLean, S. A. Bowring, Engineering cyber infrastructure for U–Pb
516 geochronology: Tripoli and U–Pb_Redux. *Geochem. Geophys. Geosyst.* **12**, Q0AA19 (2011).
517 59. P. Vermeesch, IsoplotR: a free and open toolbox for geochronology. *Geosci. Front.* **9**, 1479–
518 1493 (2018).
519 60. J. L. Kirschvink, The least-squares line and plane and the analysis of palaeomagnetic data.
520 *Geophys. J. R. Astron. Soc.* **62**, 699–718 (1980).
521 61. R. Fisher, Dispersion on a sphere. *Proc. R. Soc. A, Math. Phys. Eng. Sci.* **217**, 295–305
522 (1953).
523 62. C. H. Jones, User-driven integrated software lives: "Paleomag" paleomagnetics analysis on
524 the Macintosh. *Comput. Geosci.* **28**, 1145–1151 (2002).
525 63. L. Tauxe, R. Shaar, L. Jonestrask, N. L. Swanson-Hysell, R. Minnett, A. A. P. Koppers, C.
526 G. Constable, N. Jarboe, K. Gaastra, L. Fairchild, PmagPy: software package for

paleomagnetic data analysis and a bridge to the Magnetics Information Consortium (MagIC) Database. *Geochem. Geophys. Geosyst.* **17**, 2450–2463 (2016).
64. J. Zhang, T. Ye, Y. Dai, J. Chen, H. Zhang, C. Dai, G. Yuan, K. Jiang, Provenance and tectonic setting transition as recorded in the Neoproterozoic strata, western Jiangnan Orogen: Implications for South China within Rodinia. *Geosci. Front.* **10**, 1823-1839 (2019).
65. J. Yao, L. Shu, P. A. Cawood, G. Zhao, Differentiating continental and oceanic arc systems and retro-arc basins in the Jiangnan orogenic belt, South China. *Geological Magazine*, 1–16 (2019).
66. G.-Y. Song, X.-Q. Wang, X.-Y. Shi, G.-Q. Jiang, New U-Pb age constraints on the upper Banxi Group and synchrony of the Sturtian glaciation in South China. *Geosci. Front.* **8**, 1161–1173 (2017).
67. Bureau of Geology and Mineral Resources of Guizhou Province, Regional Geology of Guizhou Province. *Geological Publishing House, Beijing* (in Chinese with English abstract) (1987).
68. J.-H. Zhao, M.-F. Zhou, D.-P. Yan, Reappraisal of the Ages of Neoproterozoic Strata in South China: No Connection with the Grenvillian Orogeny. *Geology* **39**, 299–302 (2011).
69. M. Wang, C.-G. Dai, X.-H. Wang, H.-Z. Ma, C.-L. Peng, K.-D. Yang, Sedimentation age of the Fanjingshan Group in East Guizhou Province: evidence from in-situ zircon LA-ICP-MS U-Pb dating. *Acta Petrologica et Mineralogica* **31**, 843–857 (in Chinese with English abstract) (2012).
70. L.-Z. Gao, J.-S. Chen, C.-G. Dai, X.-Z. Ding, X.-H. Wang, Y.-X. Liu, M. Wang, H. Zhang, SHRIMP zircon U-Pb dating of tuff in Fanjingshan Group and Xiajiang Group from Guizhou and Hunan Provinces and its stratigraphic implications. *Geol. Bull. China* **33**, 949–959 (in Chinese with English abstract) (2014).
71. C. Yan, L. Shu, M. Faure, Y. Chen, R. Huang, Time constraints on the closure of the Paleo–South China Ocean and the Neoproterozoic assembly of the Yangtze and Cathaysia blocks: Insight from new detrital zircon analyses. *Gondwana Res.* **73**, 175–189 (2019).
72. L. Tauxe, G. S. Watson, The fold test: An eigen analysis approach. *Earth Planet. Sci. Lett*. **122**, 331–341 (1994).
73. J. G. Meert, A. F. Pivarunas, D. A. D. Evans, S. A. Pisarevsky, L. J. Pesonen, Z. X. Li, S. Å Elming, S. R. Miller, S. Zhang, J. M. Salminen, The magnificent seven: a proposal for modest revision of the Van der Voo (1990) quality index. *Tectonophysics* **790**, (2020).
74. G. S. Watson, Large sample theory of the Langevin distribution, *J. Stat. Plann. Inference* **8**, 245–256 (1983).
75. R. R. Doell, Paleomagnetic secular variation study of lavas from the Massif central, France. *Earth Planet. Sci. Lett.* **8**, 352–362 (1970).
76. Efron, B., The Jackknife, the Bootstrap and Other Resampling Plans. *Vermont, Capital City Press*, 93 (1982).
77. P. L. McFadden, R. T. Merrill, M. W. McElhinny, S. Lee, Reversals of the Earth's magnetic field and temporal variations of the dynamo families. *J. geophys. Res.,* **96,** 3923–3922 (1991).
78. X.-L. Wang, J.-C. Zhou, W.-L. Griffin, G. Zhao, J.-H. Yu, J.-S. Qiu, Y.-J. Zhang, G.-F. Xing, Geochemical zonation across a Neoproterozoic orogenic belt: Isotopic evidence from granitoids and metasedimentary rocks of the Jiangnan orogen, China. *Precambrian Res.* **242**, 154–171 (2014).

79. P. L. McFadden, M. W. McElhinny, The combined analysis of remagnetization circles and direct observations in palaeomagnetism. *Earth Planet. Sci. Lett.* **87**, 161–72 (1988).
80. D. F. Argus, R. S. Gross, An estimate of motion between the spin axis and the hotspots over the past century, *Geophys. Res. Lett.* **31** (2004).
81. J. X. Mitrovica, J. Wahr, Ice Age Earth rotation. *Annu. Rev. Earth Planet. Sci.* **39**, 577–616 (2011).
82. N.-H Chan, J. X. Mitrovica, I. Matsuyama, K. Latychev, J. R. Creveling, The rotational stability of a convecting Earth: the Earth's figure and TPW over the last 100 Myr. *Geophys. J. Int.* **187**, 773–82 (2011).
83. B. Steinberger, M. L. Seidel, T. H. Torsvik, Limited true polar wander as evidence that Earth's nonhydrostatic shape is persistently triaxial. *Geophys. Res. Lett*. **44**, 827–834 (2017).
84. R. N. Mitchell, C. J. Thissen, D. A. Evans, S. P. Slotznick, R. Coccioni, T. Yamazaki, J. L. Kirschvink, A Late Cretaceous true polar wander oscillation. *Nat. Commun **12***, 1–8 (2021).
85. R. R. Fu, D. V. Kent, Anomalous Late Jurassic motion of the Pacific Plate with implications for true polar wander, *Earth Planet. Sci. Lett* **490**, 20–30 (2018).
86. G. Muttoni, D. V. Kent, Jurassic monster polar shift confirmed by sequential paleopoles from Adria, promontory of Africa. *J. Geophys. Res. Solid Earth* **124**, 3288–3306 (2019).
87. R. R. Fu, D. V. Kent, S. R. Hemming, P. Gutiérrez, J. R. Creveling, Testing the occurrence of Late Jurassic true polar wander using the La Negra volcanics of northern Chile. *Earth Planet. Sci. Lett.* **529**, 15835 (2020).
88. R. Van der Voo, True polar wander during the middle Paleozoic?. *Earth Planet. Sci. Lett.* **122**, 239–243 (1994).
89. J. L. Kirschvink, R. L. Ripperdan, D. A. Evans, Evidence for a large-scale Early Cambrian reorganization of continental masses by inertial interchange true polar wander. *Science* **277**, (1997).
90. R. N. Mitchell, D. A. D. Evans, T. M. Kilian, Rapid Early Cambrian rotation of Gondwana, *Geology* **38**, 755–758 (2010).
91. R. N. Mitchell, T. D. Raub, S. C. Silva, J. L. Kirschvink, Was the Cambrian Explosion both an Effect and an Artifact of True Polar Wander? *Am. J. Sci.* **315**, 945–957 (2015).
92. R. K. Bono, J. A. Tarduno, F. Nimmo, R. D. Cottrell, Young inner core inferred from Ediacaran ultra-low geomagnetic field intensity. *Nat. Geosci.* **12**, 143–147 (2019).
93. V. V. Shcherbakova, V. G. Bakhmutov, D. Thallner, V. P. Shcherbakov, G. V. Zhidkov, A. J. Biggin, Ultra-low palaeointensities from East European Craton, Ukraine support a globally anomalous palaeomagnetic field in the Ediacaran. *Geophys. J. Int.* **220**, 1928–1946 (2020).
94. F. A. Macdonald, M. D. Schmitz, J. L. Crowley, C. F. Roots, D. S. Jones, A. C. Maloof, J. V. Strauss, P. A. Cohen, D. T. Johnston, D. P. Schrag, Calibrating the Cryogenian. *Science*, **327**, 1241–1243 (2010).
95. Y. Park, N. L. Swanson-Hysell, S. A. MacLennan, A. C. Maloof, M. Gebreslassie, M. M. Tremblay, B. Schoene, M. Alene, E. S. C. Anttila, T. Tesema, B. Haileab, The lead-up to the Sturtian Snowball Earth: Neoproterozoic chemostratigraphy time-calibrated by the Tambien Group of Ethiopia. *GSA Bulletin* **132**, 1119–1149 (2019).
96. X. Jing, Z. Yang, D. A. D. Evans, Y. Tong, Y. Xu, H. Wang, A pan-latitudinal Rodinia in the Tonian true polar wander frame. *Earth Planet. Sci. Lett.* **530**, 115–880 (2019).
97. C. Maijer, R. H. Verschure, Petrology and isotope geology of the Hunnedalen monzonoritic dike swarm, SW Norway: the Hunnedalen dike swarm as a possible late expression of Egersund anorthosite magmatism, Norges Geol. Undersøk. Bull **434**, 83–104 (1998).

98. I. M. Gorokhov, T. S. Zaitseva, A. B. Kuznetsov, G. V. Ovchinnikova, M. M. Arakelyants, V. P. Kovach, G. V. Konstantinova, T. L. Turchenko, I. M. Vasil'eva, Isotope Systematics and Age of Authigenic Minerals in Shales of the Upper Riphean Inzer Formation, South Urals. *Stratigr. Geol. Correl.* **27**, 133–158 (2019).
99. H.-Q. Zhao, S.-H Zhang, J.-K. Ding, L.-X. Chang, Q. Ren, H.-Y. Li, T.-S. Yang, H.-C. Wu, New geochronologic and paleomagnetic results from early Neoproterozoic mafic sills and late Mesoproterozoic to early Neoproterozoic successions in the eastern North China Craton, and implications for the reconstruction of Rodinia. *GSA Bulletin* **132**, 739–766 (2020).
100. A. H. Jaffey, K. F. Flynn, L. E. Glendenin, W. C. Bentley, A. M. Essling, Precision measurement of half-lives and specific activities of ^{235}U and ^{238}U. *Phys. Rev. C* **4**, 1889–1906 (1971).
101. S. Zhang, H. Li, G. Jiang, D. A. D. Evans, J. Dong, H. Wu, T. Yang, P. Liu, Q. Xiao, New paleomagnetic results from the Ediacaran Doushantuo Formation in South China and their paleogeographic implications. *Precambrian Res.* **259**, 130–142 (2015).
102. S. Zhang, D. A. D Evans, H. Li, H. Wu, G. Jiang, J. Dong, Q. Zhao, T. D. Raub, T. S. Yang, Paleomagnetism of the late Cryogenian Nantuo Formation and paleogeographic implications for the South China Block. *J. Asian Earth Sci.* **72**, 164–177 (2013).
103. X. Jing, Z. Yang, Y. Tong, Z. Han, A revised paleomagnetic pole from the mid-Neoproterozoic Liantuo Formation in the Yangtze block and its paleogeographic implications. *Precambrian Res.* **268**, 194–211 (2015).
104. X. Jing, D. A. D. Evans, Z. Yang, Y. Tong, Y. Xu, H. Wang, Inverted south China: A novel configuration for Rodinia and its breakup. *Geology* **49**, 463–467 (2021).
105. J. Niu, Z.-X. Li, W. Zhu, Palaeomagnetism and geochronology of mid- Neoproterozoic Yanbian dykes, South China: implications for a c. 820–800 Ma true polar wander event and the reconstruction of Rodinia. *Geol. Soc. (Lond.) Spec. Publ.* **424**, 191–211 (2016).
106. B.-C. Huang, Y.-X. Zhou, R.-X. Zhu, Discussions on Phanerozoic evolution and formation of continental China, based on paleomagnetic studies. *Earth Sci. Front.* **15**, 348–359 (2008).
107. R. J. Enkin, Z. Yang, Y. Chen, V. Courtillot, Paleomagnetic constraints on the geodynamic history of the major blocks of China from the Permian to the present. *J. Geophys. Res.: Solid Earth* **97**, 13953–13989 (1992).
108. X. Zhao, R. S. Coe, S. A. Gilder, G. M. Frost, Palaeomagnetic constraints on the palaeogeography of China: implications for Gondwanaland. *Aust. J. Earth Sci.* **43**, 643–672 (1996).
109. H.-N. Wu, R.-X. Zhu, L.-X. Bai, B. Guo, J.-J. Lü, Revised apparent polar wander path of the Yangtze Block and its tectonic implications. *Sci. China Ser. D: Earth Sci.* **41**, 78–90 (1998).
110. S. Zhang, H. Zhu, X. Meng, New paleomagnetic results from the Devonian-Carboniferous successions in the Southern Yangtze Block and their paleogeographic implications. *Acta Geol. Sin.* **75**, 303–313 (2001).
111. H. Xian, S. Zhang, H. Li, Q. Xiao, L. Chang, T. Yang, H. Wu, How did south China connect to and separate from Gondwana? New paleo- magnetic constraints from the Middle Devonian red beds in south China. *Geophys. Res. Lett.* **46**, 7371–7378 (2019).
112. N. D. Opdyke, K. Huang, G. Xu, W.-Y. Zhang, D. V. Kent, Paleomagnetic results from the Silurian of the Yangtze paraplatform. *Tectonophysics* **139**, 123–132 (1987).

113. K. Huang, N. D. Opdyke, R. X. Zhu, Further paleomagnetic results from the Silurian of the Yangtze Block and their implications. *Earth Planet. Sci. Lett.* **175**, 191–202 (2000).
114. Z. Yang, Z. Sun, T. Yang, J. Pei, A long connection (750–380 Ma) between South China and Australia: paleomagnetic constraints. *Earth Planet. Sci. Lett.* **220**, 423–434 (2004).
115. J.-L Lin, M. Fuller, W.-Y. Zhang, Paleogeography of the north and south China blocks during the Cambrian. *J. Geodyn.* **2**, 91–114 (1985).
116. D.A.D. Evans, The palaeomagnetically viable, long-lived and all-inclusive Rodinia supercontinent reconstruction. *Geol. Soc. (Lond.) Spec. Publ.* **327**, 371–404. (2009).
117. D. A. D. Evans, R. V. Veselovsky, P.Y. Petrov, A.V. Shatsillo, V. E. Pavlov, Paleomagnetism of Mesoproterozoic margins of the Anabar Shield: A hypothesized billion-year partnership of Siberia and northern Laurentia. *Precambrian Res.* **281**, 639–655 (2016).
118. J. Ding, S. Zhang, D. A. D. Evans, T. Yang, H. Li, H. Wu, J. Chen, North China craton: The conjugate margin for northwestern Laurentia in Rodinia. *Geology* **49**, 773–778 (2021).
119. Z.-X. Li, D. A. D. Evans, Late Neoproterozoic 40° intraplate rotation within Australia allows for a tighter-fitting and longer-lasting Rodinia. *Geology* **39**, 39–42 (2011).

Acknowledgments:

We thank N. L. Swanson-Hysell, F. A. Macdonald, Y. Park, Q. Ren, H. Zhao and Z. Chen for the help with field work and samplings. We thank Y. Xu for the assistance with thermal demagnetization of specimens; B. E. Hodgin, J. Pu, and A. Eyster for the help with mineral separations; J. Ding, L. Zhang, J. Dong, L. Zeng, and S. B. Jacobsen for valuable discussions. We especially thank F. A. Macdonald and N. L. Swanson-Hysell for helpful suggestions and edits that improved the original manuscript. We thank K. Hodges for the careful editorial handling of our manuscript. We also thank J. L. Kirschvink, R. N. Mitchell, and an anonymous reviewer for insightful reviews that improved the manuscript. Finally, we thank Fanjingshan World Natural Heritage Administration for the permission to sample. **Funding:** This study was supported by National Natural Science Foundation of China Grant 41830215 and the "111"project (B20011), both to S. Zhang. **Author contributions:** S. Z. and H. F. designed the research. H. F., S. Z., D. J. C., and H. X. conducted the study. H. F. and S. Z. drafted and finalized the manuscript. All authors reviewed the manuscript and provided comments. **Competing interests:** The authors declare no known competing interests. **Data and materials availability:** All data needed to evaluate the conclusions in the paper are present in the paper and/or the Supplementary Materials. Codes used for analysis and measurement-level paleomagnetic data are available on Zenodo at https://doi.org/10.5281/zenodo.6647160 and GitHub at https://github.com/fuhairuo/Fanjingshan-Sills. The data will also be posted in the Magnetics Information Consortium (MagIC) database (www2.earthref.org/MagIC/).

Supplementary Materials:

Supplementary Text
Figs. S1 to S15
Tables S1 to S8